

Multimodal Continual Learning with MLLMs from Multi-scenario Perspectives

Kai Jiang^{1,2*}, Sisi Huang^{1,2*}, Xiangyu Chen², Jiawei Shao², Hongyuan Zhang^{2,3†}, Xuelong Li^{2†}

¹School of Artificial Intelligence, OPTics and ElectroNics, Northwestern Polytechnical University

²Institute of Artificial Intelligence (TeleAI) of China Telecom

³University of Hong Kong

jk@mail.nwp.edu.cn, 4777huang@gmail.com, chxy95@gmail.com,
jiawei.shao@connect.ust.hk, hyzhang98@gmail.com, xuelong.li@ieee.org

Abstract

Continual learning in visual understanding aims to deal with catastrophic forgetting in Multimodal Large Language Models (MLLMs). MLLMs deployed on devices have to continuously adapt to dynamic scenarios in downstream tasks, such as variations in background and perspective, to effectively perform complex visual tasks. To this end, we construct a multimodal visual understanding dataset (MSVQA) encompassing four different scenarios and perspectives including high altitude, underwater, low altitude and indoor, to investigate the catastrophic forgetting in MLLMs under the dynamics of scenario shifts in real-world data streams. Furthermore, we propose *mUltimodal coNtinual learning with MLLMs From multi-scenario pERspectives* (UNIFIER) to address visual discrepancies while learning different scenarios. Specifically, it decouples the visual information from different scenarios into distinct branches within each vision block and projects them into the same feature space. A consistency constraint is imposed on the features of each branch to maintain the stability of visual representations across scenarios. Extensive experiments on the MSVQA dataset demonstrate that UNIFIER effectively alleviates forgetting of cross-scenario tasks and achieves knowledge accumulation within the same scenario.

1. Introduction

Real-world data streams are typically collected by various devices across different regions, implying that they often encompass diverse perspectives and environments. Consequently, multimodal large models (MLLMs) deployed on devices are constrained by the scale of parameters, necessitating continuous adaptation to scenario shifts in real-world

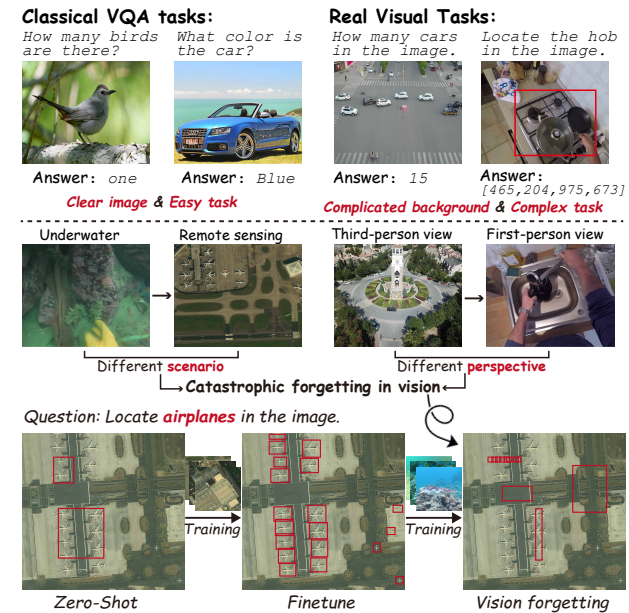


Figure 1. **Task comparison and vision forgetting.** Classical settings focus on parsing of user intent from text. In real visual tasks, the image background is more complex and the task is more challenging. Untrained model cannot precisely predict the bounding bbox while finetuning with the corresponding scenario can address the issue. But learning a new scenario results in vision forgetting (Severe false positives and false negatives).

applications. However, this scenario shift leads to catastrophic forgetting [10, 25, 54], where models tend to overfit the current scenario and forget the old one. To this end, continual learning [8, 19, 31, 33, 40] aims to learn a unified model from a data stream. It requires the model to learn the training data in sequence without accessing the previous data. Ultimately, the model should achieve the same performance as training a model with all data. Despite significant advances in continual learning, most existing works focus on unimodal tasks such as image classification [20, 23, 29, 51]. For real-world applications, it should

*These authors contributed equally to this work

†Corresponding authors

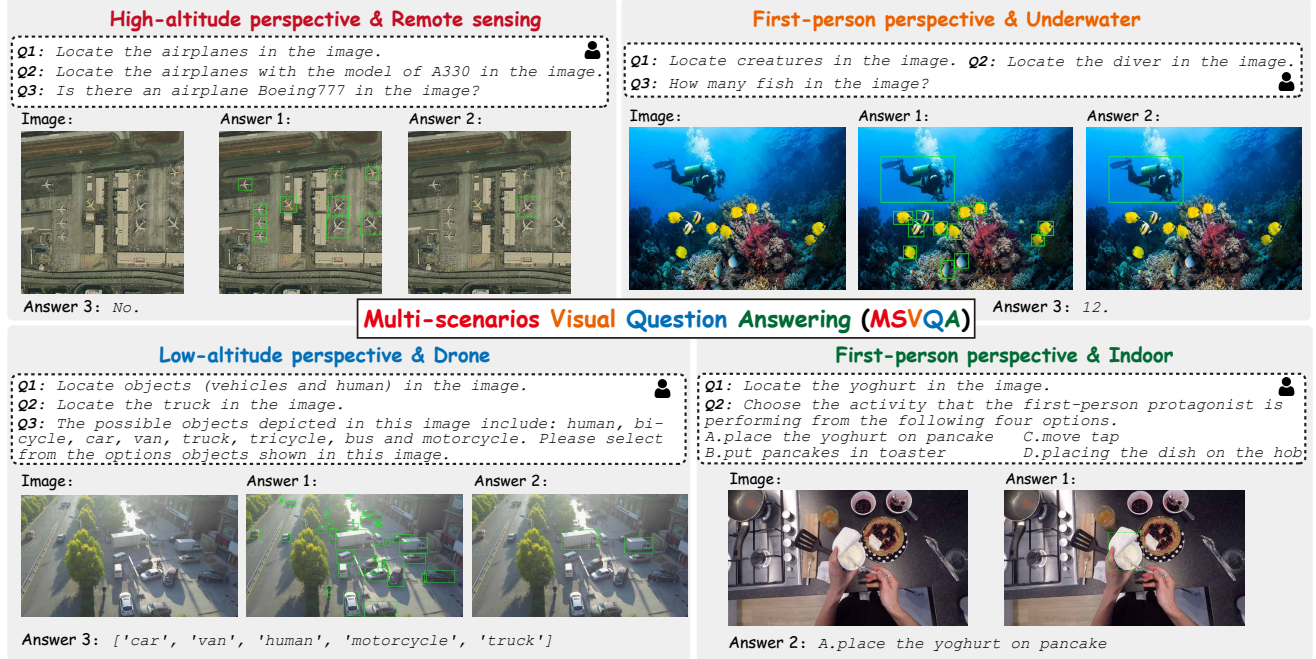


Figure 2. Examples of some image-text pair in the MSVQA dataset. **More details are provided in the supplementary materials.**

develop multimodal learning [21, 46, 48, 55] to integrate complex visual and textual reasoning.

Multimodal understanding [2, 13, 14, 26, 27] requires the model to understand the user intent, to extract relevant information from the image, and to generate text for the response. The inherent modal conflicts exacerbate catastrophic forgetting in continual learning [45]. Both textual and visual representations are prone to overlapping. However, existing works primarily focus on the forgetting of textual modality but lack attention to visual modality [32, 49]. For instance, most VQA datasets are composed of the same scenarios and similar perspectives, and the questions are simple, such as asking about the color or quantity of an object. For the classical setting [49], the core challenge lies in the accurate parsing of user intent from text.

However, the classical setting neglects **complicated backgrounds** and **complex demands** in vision tasks. As illustrated in Fig. 1, an image from a normal working device usually contains a large number of objects. The key vision information occupies only a small region of the complex background. And visual tasks usually involve complex requirements, such as identifying the coordinates or types of a particular target, rather than some general information. **Extracting fine-grained information from the complex background** constitutes the core challenge of vision tasks. The real-world data streams usually develop different scenarios and different perspectives as the environment and equipment change. The shift of scenarios or perspectives affects the tendency of the model to extract visual informa-

tion, which leads to catastrophic forgetting for MLLMs.

To this end, we **construct a Multi-Scenario Visual Question Answering (MSVQA) dataset to evaluate the forgetting of continual learning** in the shifts of scenarios or perspectives. Fig. 2 shows some examples in the MSVQA datasets. It mainly consists of four different scenarios and perspectives with each scenario may change according to the location and time. In different scenarios, the size and density of objects vary widely. Variations in lighting conditions and occlusions within complex environments increase the difficulty of MSVQA. Therefore, **the dataset enables the simulation of a more realistic real-world data flow**. More details are provided in the supplementary material.

During learning in cross-scenario data streams, the model acquires different vision representations in each scenario. This results in deviations to interpret the image from previous scenarios after learning a new scenario. For example, when transitioning from a dense prediction scenario to a target-sparse one, the model misjudges the size and quantity of targets, causing a high incidence of false positives and false negatives. This discrepancy in the parsing of visual information constitutes one of the contributing factors to catastrophic forgetting in MLLMs. Therefore, we propose **mUltimodal coNtinual learning with MLLMs** From multi-scenario pERspectives (UNIFIER) to align the vision representations across different scenarios. Specifically, it learns each new scenario by expanding a branch within the vision block. The features of all branches are concatenated into

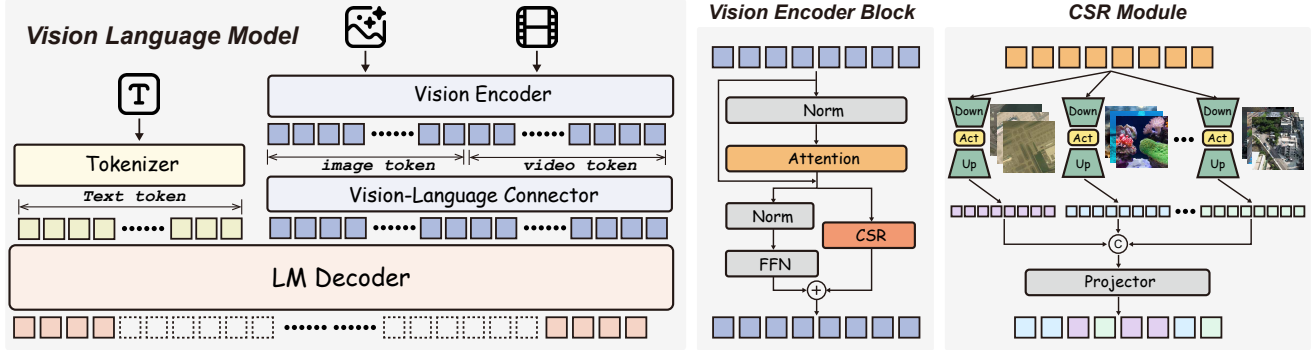


Figure 3. The overview of UNIFIER. The left denotes a standard structure of a VLM. The middle denotes the details of the vision block in UNIFIER. The right denotes CSR module, which is added only on the vision encoder to isolate parameters for different scenarios.

a feature vector and projected to a shared feature space to merge with the features from pre-trained vision backbone. Then, different vision representations across scenarios are constrained by a consistent loss between branches and between the new and old models. The main contributions of our work are three-fold:

- We propose the MSVQA dataset and a corresponding continual learning benchmark in MLLMs to evaluate catastrophic forgetting of vision representations under complex scene variations.
- We propose mUltimodal coNtinual learning From multi-scenario pERspectives (UNIFIER) to align the vision representations across different scenarios. It learns each scenario with a new branch within vision blocks and constrains the features of different scenarios to obtain consistent vision representations, thereby reducing catastrophic forgetting caused by scenario alterations.
- Extensive experiments validated on the MSVQA dataset demonstrate that our approach can alleviate the catastrophic forgetting when learning different scenarios for MLLMs, which improves the last-step F1 score by 3.4%~7.69% in the setting of 20 steps compared to the state-of-the-art approach.

2. Related Works

Multimodal Large Language Models extend the capabilities of traditional large language models (LLMs) to process and understand multimodal information. They are inspired by representation learning [4, 12, 18, 47] such as CLIP [14, 17, 35] and integrate specialized encoders to convert various modal inputs to a unified representation. Then, LLMs integrate these unified representations from various modalities and perform complex multimodal reasoning. Existing models such as QwenVL [41] and LLaVA [30] have demonstrated that LLMs can handle multimodal information after modal alignment. In this paper, we develop the capabilities of MLLMs in continual learning, to understand

new scenarios and respond correctly.

Continual Learning for MLLMs aims to develop the capabilities of MLLMs to acquire new data and skills without forgetting. The basic and key challenge lies in catastrophic forgetting due to representation overlap and parameter drift. Some classical CL approaches [22, 24] penalize parameter drift by restricting the update of key parameters [1] with loss function. Following the same principle, Model Tailor [52] randomly removes updates for most parameters after finetuning and amplifies those for the remaining parameters. Inspired by representation learning, VQACL [49] introduces a sample-specific and a sample-invariant feature to learn a discriminative and generalizable representation. Inspired by the distillation [28] and rehearsal [36] approaches, QUAD [32] only saves all previous questions and uses intermediate attention [38] of querying the new image with the old questions for distillation. Although it alleviates forgetting in text modality, the visual discrepancies are ignored across different scenarios.

3. Methodology

Motivation and overview It is a natural scheme to learn a *single* LoRA[15] branch, but it still suffers from severe catastrophic forgetting if we adapt on-device MLLMs to *multiple* scenarios. Therefore, learning multiple LoRA branches to isolate the parameters is an intuitive way to tackle this challenge. However, it also encounters the issue of selecting the correct route. Furthermore, the gating network also encounters catastrophic forgetting if used to select the correct branch, especially without saving previous data. To deal with multiple scenarios while avoiding the need of routing, we propose Vision Representation Expansion (VRE) in Sec. 3.2 to isolate the parameters for each scenario and then project their representations into a unified feature space. To further avoid drift for new representations, we propose Vision Consistency Constraint (VCC) in Sec. 3.3 to align the intermediate representation

of branches. Detailed ablation experiments demonstrate that **VRE outperforms the simple multi-branch (multi-LoRA) one**, and VCC works better on resisting representation drift than strict constraints.

3.1. Problem Setup

Assume a real-world data stream comprising T tasks, denoted as $\mathcal{D} = \{\mathcal{D}_1, \mathcal{D}_2, \dots, \mathcal{D}_T\}$, with each task data $\mathcal{D}_t = \{(x_i^t, q_i^t, y_i^t)\}_{i=1}^{n_t}$ collected from different scenarios (e.g., indoor or outdoor) using task-specific methods, such as varying devices and perspectives. $x_i^t \in \mathcal{X}_t$ is the input image, $q_i^t \in \mathcal{Q}_t$ the question, and $y_i^t \in \mathcal{Y}_t$ the corresponding answer. The model is required to learn the current task data \mathcal{D}_t without forgetting the previous data $\{\mathcal{D}_1, \mathcal{D}_2, \dots, \mathcal{D}_{T-1}\}$.

In comparison to the classical setting, this setting introduces the challenge of scenario shift. Cross-scenario tasks require that the model have to **learn the complex vision information in the new scenario** rather than **simply reusing the visual abilities** developed in previous tasks. The model should continuously retain the learned knowledge and **perform increasingly better in the same scenario**. After learning the whole data stream, it is validated on the test set of all scenarios and required to exhibit a performance equivalent to training the model using all data.

3.2. Vision Representation Expansion

Scenario alteration in the real-world data stream requires the MLLMs deployed on devices to learn new representations without forgetting previous ones. Although we can store all textual questions [32], it is impractical to store all images or videos. And visual data has a lower information density and is frequently contaminated with significant noise and irrelevant content. This can lead to overlapping and drifting visual representations when learning different vision data across scenarios, thereby causing catastrophic forgetting. Fig. 1 shows an example of forgetting in the vision representation for MLLMs. Untrained MLLM cannot respond to the user correctly. As illustrated in Fig. 1, **relying solely on visual priors tends to lose fine-grained information**, resulting in the omission of small targets. After fine-tuning, the model can locate the target precisely. However, the model cannot correctly extract the visual features of the old scenarios after learning new scenarios. It is caused by the vision representation overlap. The visual representations of old and new scenarios exhibit significant differences, and the representations learned from new scenarios hinder the feature extraction from old scenarios.

Accordingly, our goal is to **decouple visual representations for different scenarios** in the training process. This process must account for the actual data acquisition conditions, where training data for a single task is typically collected from the same environment, while the test environ-

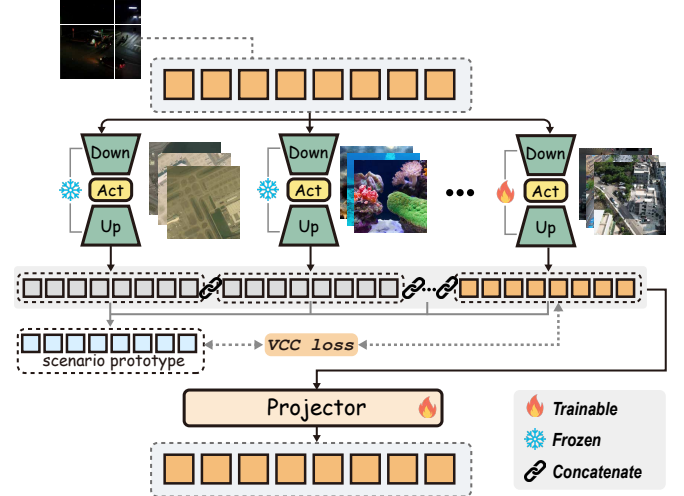


Figure 4. Training illustration of CSR module. Only one branch is involved in the training for a new scenario. The VCC loss constraint ensures consistency in the representations across various scenarios.

ment is unknown. Inspired by dynamic architecture models [16, 23, 44], visual information from different scenarios can be isolated in different model parameters. However, expanding the entire backbone is only feasible for small models and is not suitable for MLLMs. Training with PEFT methods to expand a LoRA branch to learn each task [50] also leads to a multiplicative increase in computational overhead during inference.

Therefore, we propose vision representation expansion (VRE) to decouple visual representations for different scenarios without increasing computational load in both training and inference. As illustrated in Fig. 3, a vision-language model consists mainly of a vision encoder and a text encoder. The vision encoder extracts the features of images or videos and then the features are projected on the textual feature space to align with the text embeddings. Thus, new parameters can be expanded in the vision encoder to learn new scenario representations to achieve the isolation of visual information. Assume that a vision encoder $\mathcal{F}_v = \{f_1, \dots, f_L\}$ consists of L vision blocks f_l , the forward propagation of the vision encoder can be represented as

$$r_1 = f_1(x_i^t), \quad (1)$$

$$r_l = f_l(r_{l-1}). \quad (2)$$

Each vision block usually consists of an attention module A_l and an FFN layer s_l . A cross-scenario representation (CSR) module is inserted into the vision block and performs parallel inference with the FFN layer. Then, the

visual block can be formulated as

$$a_l = A_l (\text{LN}(r_{l-1})) + r_{l-1}, \quad (3)$$

$$r_l = s_l (\text{LN}(a_l)) + p_l, \quad (4)$$

where p_l is the output of the CSR module and LN is the layer normalization. It consists of multiple branches and a projector to separate different scene information and project them onto the same feature space. It can be represented as

$$p_l = \mathcal{P}_l (\varphi_l^1(a_l) \oplus \dots \oplus \varphi_l^K(a_l)), \quad (5)$$

$$\varphi(\cdot) = \phi_{\text{up}}(o(\phi_{\text{down}}(\cdot))), \quad (6)$$

where K denotes the number of scenarios, $\mathcal{P}_l \in \mathbb{R}^{K \times d_1 \rightarrow d_1}$ denotes the projector to integrate all representations of various scenarios, ϕ_{down} denotes the down-projection layer, ϕ_{up} denotes the up-projection layer and o denotes the activation function. $\phi_{\text{down}} \in \mathbb{R}^{d_1 \rightarrow d_2}$ reduces the dimension of the input feature vector from d_1 to d_2 , while $\phi_{\text{up}} \in \mathbb{R}^{d_2 \rightarrow d_1}$ restores it to d_1 , where $d_1 \gg d_2$. As illustrated in Fig. 4, only one branch is trainable in the training of the new scenario, while the parameters of other branches remain frozen.

3.3. Vision Consistency Constraint

Although we reduce the mutual interference of visual information among different scenarios through parameter isolation, **directly learning new scenarios fails to constrain internal representation** [34, 42], leading to **feature drift** and **destroying the consistency of representations** across tasks. This inconsistency shifts self-attention [11, 23, 39], thus the model focuses on an irrelevant visual region to previous scenarios. Some distillation-based CL approaches maintain cross-task consistency by comparing intermediate representations of the new and old models [3, 9, 43]. These explicit regularization methods are proven to be effective in aligning internal representations. However, this strict constraint within the layers limits the plasticity of the model [32]. Especially for images of an unseen scenario, it fails to learn new scenario representations if aligning the intermediate features using strict regularization due to the lack of visual prior. Therefore, maintaining the representation consistency across different scenarios without compromising the model plasticity lies a challenge to learn a new vision representation in continual learning.

To address these challenges, it learns a consistency constraint within the CSR module in each vision block of the model to **learn a consistent vision representation in different scenarios**. Due to the multi-branch structure, which retains visual scenario information from previous tasks, it can **align the representations of different branches** without distillation between models. Specifically, scenario-specific vision representations are reserved in φ_l^k . For a random scenario input, K different vision features $\{\varphi_l^1(a_l), \dots, \varphi_l^K(a_l)\}$ can be obtained. We can calculate

a scenario prototype μ_l as an explicit multi-scenario unified representation, and then align the representations of each branch with this prototype.

$$\mu_l = \frac{1}{K} \sum_{k=1}^K \varphi_l^k(a_l) \quad (7)$$

The simplest way constrains the representations of all branches by the ℓ^2 -distance between scenario prototype $\mu_l \in \mathbb{R}^{\text{seq} \times d_1}$ and the representation $\varphi_l^k(a_l) \in \mathbb{R}^{\text{seq} \times d_1}$, resulting in the lowest model plasticity. Similarly to knowledge distillation, we compute the relative entropy using soft labels as a constraint instead of ℓ^2 -distance. By computing the mean vectors $\bar{\varphi}_l^{\text{fe}}(a_l) \in \mathbb{R}^{d_1}$ and $\bar{\varphi}_l^{\text{em}}(a_l) \in \mathbb{R}^{\text{seq}}$ along the feature and embedding channels, we aim to penalize the global changes of representations and allow them to reorganize across the channels:

$$\mathcal{L}_c^{l,k} = \text{KL} \left(\frac{\bar{\varphi}_l^{k,\text{fe}}}{\tau} \middle| \frac{\bar{\mu}_l^{\text{fe}}}{\tau} \right) + \text{KL} \left(\frac{\bar{\varphi}_l^{k,\text{em}}}{\tau} \middle| \frac{\bar{\mu}_l^{\text{em}}}{\tau} \right), \quad (8)$$

where $\bar{\mu}_l^{\text{fe}}$ and $\bar{\mu}_l^{\text{em}}$ denote the mean vectors of the scenario prototype μ_l along the feature and embedding channels, τ the distillation coefficient, and $\text{KL}(\cdot | \cdot)$ the relative entropy. To prevent parameter drift of projectors, we align the intermediate representations p_l of both the old and new models in the same manner as in Eq. (9),

$$\mathcal{L}_p^l = \text{KL} \left(\frac{\bar{p}_l^{\text{fe},\text{new}}}{\tau} \middle| \frac{\bar{p}_l^{\text{fe},\text{old}}}{\tau} \right) + \text{KL} \left(\frac{\bar{p}_l^{\text{em},\text{new}}}{\tau} \middle| \frac{\bar{p}_l^{\text{em},\text{old}}}{\tau} \right) \quad (9)$$

where \bar{p}_l^{fe} and \bar{p}_l^{em} denote the mean vectors of p_l along the feature and embedding channels. The vision consistency constraint loss \mathcal{L}_{vcc} is obtained by the averages of $\mathcal{L}_c^{l,k}$ and \mathcal{L}_p^l in all layers:

$$\mathcal{L}_{\text{vcc}} = \frac{1}{L} \sum_{l=1}^L \left(\mathcal{L}_p^l + \sum_{k=1}^K \mathcal{L}_c^{l,k} \right). \quad (10)$$

4. Experiments

4.1. Experimental Settings

Datasets. All experiments are conducted on MSVQA datasets, which consist of 4 different scenarios, with each scenario data collected from various perspectives using different devices. The diversity of perspectives and devices forces the model to develop its visual feature extraction capability to perform well in different scenarios. Detailed information can be found in the supplementary materials.

Protocols. We split the whole dataset into T tasks, denoted as T steps. Data from each scenario is divided equally into multiple subsets and allocated to individual steps, with each step containing data from only one scenario. We set $T=5, 10$ and 20 to further investigate the performance of all

Table 1. Average and Last performance comparison with $T = 5$ on MSVQA. **Mem.** denotes the type of exemplar set, including questions (█) and images (█). **X** indicates that no data from previous tasks is saved. Best results are in **bold**, second-best are underlined.

Methods	Mem.	High altitude				Underwater				Low altitude				Indoor			
		VQA		F1		VQA		F1		VQA		F1		VQA		F1	
		\bar{A}	A_T	\bar{A}	A_T	\bar{A}	A_T	\bar{A}	A_T	\bar{A}	A_T	\bar{A}	A_T	\bar{A}	A_T	\bar{A}	A_T
Zero-shot	X	—	20.55	—	23.74	—	19.30	—	35.41	—	14.94	—	14.67	—	52.40	—	49.89
Joint	X	—	64.97	—	75.41	—	84.27	—	75.32	—	59.80	—	34.33	—	87.20	—	74.93
Finetune	X	36.35	30.09	41.45	36.36	54.08	74.98	45.62	63.50	36.44	32.27	18.51	18.01	62.00	51.40	47.99	47.84
EWC [1]	X	35.23	31.70	44.05	37.27	55.38	76.14	49.05	66.94	38.72	35.27	20.47	23.34	66.44	55.00	48.69	50.95
Tailor [52]	X	38.15	33.40	43.88	35.27	55.98	76.97	47.34	67.31	37.76	34.56	20.11	20.99	63.64	53.60	49.11	50.05
ER [5]	█ + █	50.01	43.64	64.04	58.73	68.24	78.16	54.69	68.55	49.63	48.12	24.60	22.91	67.20	61.40	54.77	55.98
PODNet [9]	█ + █	56.87	52.95	70.77	68.03	79.89	79.38	69.99	69.81	54.88	52.87	31.41	30.95	82.36	81.20	64.57	64.89
VQACL [49]	█ + █	50.42	41.22	68.02	64.71	76.22	78.60	67.09	69.29	52.58	47.21	28.50	24.65	81.70	82.00	60.21	58.95
QUAD [32]	█	57.83	56.59	71.64	70.33	80.43	79.62	70.61	70.61	54.58	52.15	31.54	31.17	82.76	82.80	65.27	63.60
UNIFIER	X	62.24	63.13	72.86	73.76	82.01	82.20	71.95	72.07	56.75	57.81	32.61	33.16	84.72	85.70	66.59	69.85
($\Delta\%$)	█	(+4.41)	(+6.54)	(+1.22)	(+3.43)	(+1.58)	(+2.58)	(+1.34)	(+1.46)	(+1.87)	(+4.94)	(+1.07)	(+1.99)	(+1.96)	(+2.90)	(+1.32)	(+4.96)

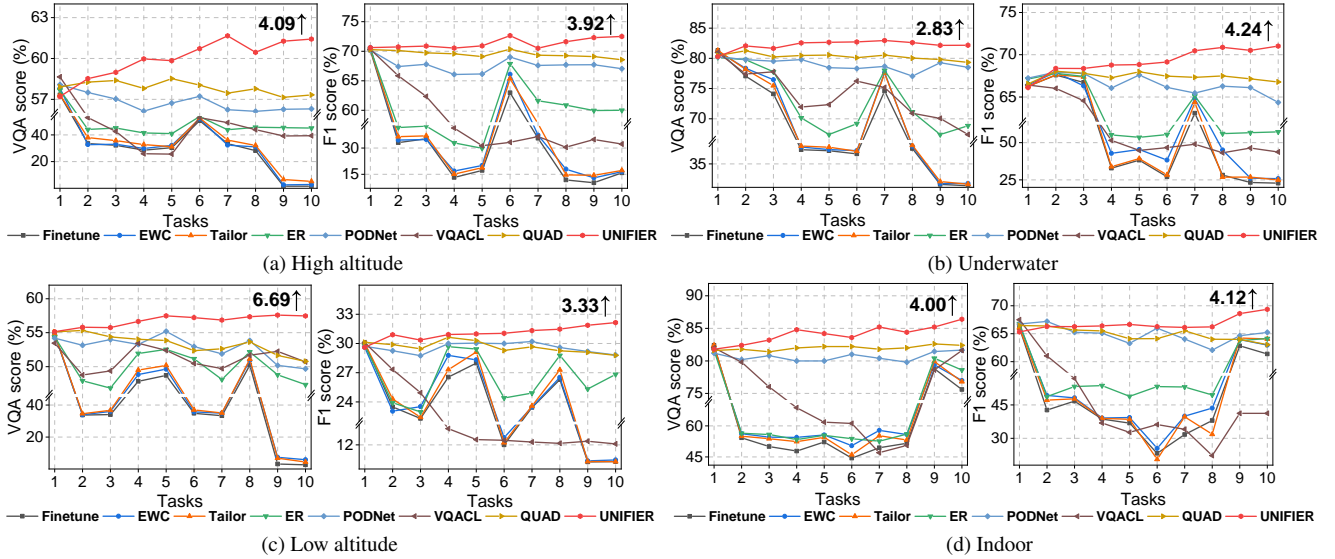


Figure 5. Incremental trends on 10 steps setting in different scenarios. The performance gap is annotated at the end of each curve.

methods at various step sizes. To prevent leakage of image information, we partition the data at the image level as opposed to the annotation level, ensuring that the images in each step are mutually exclusive. The model should learn each task in sequence and be validated in the test set of all scenarios after each step. Following previous work [23, 28, 50], the learning order is determined by random seed 1993.

Evaluation metric. We incorporate the F1 score from object detection [56] and combine it with the VQA score for a joint evaluation of MLLM performance in complex visual tasks. Following previous work, let A_t denote the VQA score or F1 score after learning the task t , we use the average performance $\bar{A} = (1/T) \sum_{t=1}^T A_t$ across T steps and the last performance A_T as metrics for continual learning. Detailed calculation procedures for all metrics are provided in the supplementary materials along with the dataset description.

Comparison methods. The proposed approach is compared with six established continual learning methods,

which consist of two rehearsal-free approaches: EWC [1] and Tailor [52], and four rehearsal-based approaches: ER [5], PODNet [9], VQACL [49], and QUAD [32]. Rehearsal-based methods are capable of storing up to 1000 images and their associated annotations. In particular, QUAD retains all the questions without storing images from old tasks. Details about these methods are provided in the supplementary materials. Furthermore, we compare the theoretical performance bounds in continual learning: the lower bound (Finetune), and the upper bound (Joint). Finetune trains the model using only current task data, whereas Joint retrains the model with all data from all seen tasks. We also report the results of zero-shot to demonstrate the necessity of fine-tuning.

Implementation details. To ensure a fair comparison, all methods are trained using the same foundation model. Given that the QwenVL series models are capable of handling complex visual tasks, including visual grounding tasks, we selected Qwen2.5VL as the foundation model. To facilitate deployment on mobile platforms, we use

Table 2. Average and Last performance comparison with $T = 20$ on MSVQA. **Mem.** denotes the type of exemplar set, including questions (❑) and images (❑). \times indicates that no data from previous tasks is saved. Best results are in **bold**, second-best are underlined.

Methods	Mem.	High altitude				Underwater				Low altitude				Indoor			
		VQA		F1		VQA		F1		VQA		F1		VQA		F1	
		\bar{A}	A_T	\bar{A}	A_T	\bar{A}	A_T	\bar{A}	A_T	\bar{A}	A_T	\bar{A}	A_T	\bar{A}	A_T	\bar{A}	A_T
Zero-shot	\times	—	20.55	—	23.74	—	19.30	—	35.41	—	14.94	—	14.67	—	52.40	—	49.89
Joint	\times	—	64.97	—	75.41	—	84.27	—	75.32	—	59.80	—	34.33	—	87.20	—	74.93
Finetune	\times	26.96	40.67	26.90	48.52	45.56	35.40	32.17	25.14	30.04	20.30	13.87	8.80	59.36	46.40	35.99	21.27
EWC [1]	\times	28.19	43.41	34.02	51.41	48.64	46.29	43.67	37.88	33.75	38.43	17.96	17.71	62.89	54.80	47.42	46.46
Tailor [52]	\times	29.00	41.62	28.00	49.77	47.86	37.87	34.32	28.03	30.34	20.80	14.34	5.04	59.91	47.40	37.13	22.40
ER [5]	❑ + ❑	45.04	45.02	53.48	58.48	70.64	65.24	56.13	50.53	49.92	46.13	25.28	24.00	64.21	66.80	56.18	61.56
PODNet [9]	❑ + ❑	48.30	49.49	64.14	63.35	75.61	76.75	63.14	62.04	52.62	52.42	28.67	27.62	79.30	79.20	62.29	64.47
VQACL [49]	❑ + ❑	42.71	48.47	31.10	25.71	75.50	74.70	42.25	35.52	51.52	51.58	12.34	7.80	70.13	78.80	34.44	32.23
QUAD [32]	❑	50.77	47.32	65.74	62.85	77.06	77.00	62.55	57.44	49.20	44.73	29.19	25.86	80.42	80.60	54.70	50.14
UNIFIER	\times	59.20	60.11	68.17	69.39	78.12	80.79	69.06	69.73	54.36	55.12	30.71	31.02	82.44	83.60	66.51	69.23
($\Delta\%$)		(+8.43)	(+10.62)	(+2.43)	(+6.04)	(+1.06)	(+3.79)	(+5.92)	(+7.69)	(+1.74)	(+2.70)	(+1.52)	(+3.40)	(+2.02)	(+3.00)	(+4.22)	(+4.76)

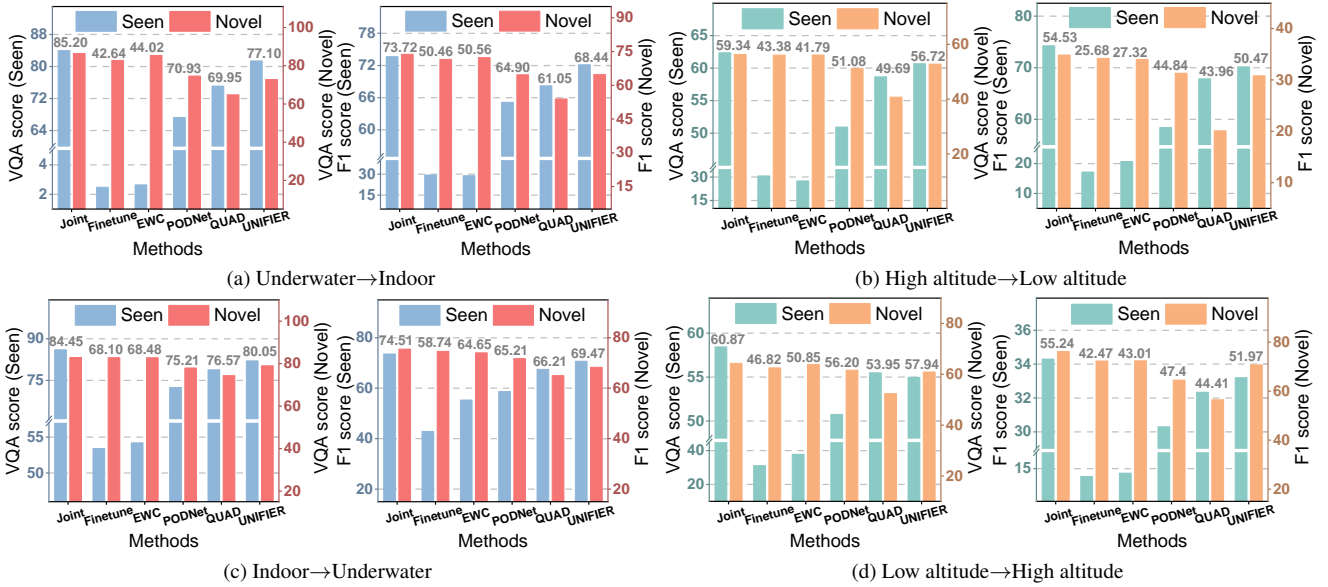


Figure 6. Performance comparison cross scenarios in one step. Average score of each method in the seen and novel scenarios is annotated on the top of each bar.

Qwen2.5VL-3B in our experiments. Following its technical report, we utilize the AdamW optimizer with an initial learning rate of 10^{-5} . A warm-up stage is added in each training phase to increase the learning rate to 0.03, and then it is decreased to 0 with a cosine annealing scheduler. The batch size is set to 64 and is allocated to 8 Nvidia H200 GPUs. For each method, the model is trained for 20 epochs in the initial task and 10 epochs in each subsequent task.

4.2. Main Results

Comparison in standard settings. Tab. 1 and Tab. 2 compare the performance in the cross-scenario of various continual learning methods in the settings of $T = 5$ and $T = 20$. The proposed approach UNIFIER achieves superior performance in both settings. It outperforms the runner-up approach by 1.58%~4.41% on the average of VQA score and by 2.58%~6.54% on the last-step VQA score in different scenarios with $T = 5$. It outperforms the runner-up approach by 1.06%~8.43% on the average of VQA score and

by 2.70%~10.62% on the last-step VQA score in different scenarios with $T = 20$. In addition, UNIFIER also performs better on complex visual tasks. It outperforms the runner-up approach by 1.07%~1.34% on the average of F1 score and by 1.46%~4.96% on the last-step F1 score in different scenarios with $T = 5$. And it outperforms the runner-up approach by 1.52%~5.92% on the average the F1 score and by 3.40%~7.69% on the last-step F1 score in different scenarios with $T = 20$. Fig. 5 shows the incremental trends in different scenarios with $T = 10$. Most compared approaches show a significant decline in performance in some steps. This indicates that **learning another scenario leads to a decline in performance on previously learned scenarios**. In contrast, UNIFIER improves its performance in another specific scenario without forgetting the previous ones. This indicates that **UNIFIER achieves knowledge accumulation** in multimodal continual learning.

Comparison of cross scenarios in one step. We further perform one-step incremental experiments to investi-

Table 3. Ablation study with $T = 10$ on MSVQA.

Methods	High altitude				Underwater				Low altitude				Indoor			
	VQA		F1		VQA		F1		VQA		F1		VQA		F1	
	\bar{A}	A_T	\bar{A}	A_T	\bar{A}	A_T	\bar{A}	A_T	\bar{A}	A_T	\bar{A}	A_T	\bar{A}	A_T	\bar{A}	A_T
Baseline	29.74	1.60	30.54	15.82	53.26	2.48	43.62	22.77	34.33	2.62	19.94	3.72	58.64	75.60	44.80	61.38
w/ VRE	51.03	51.82	53.46	54.77	75.36	74.07	56.16	55.45	52.07	48.28	25.15	24.33	81.52	82.00	61.95	62.91
w/ VRE+ ℓ^2 -dis.	53.38	53.47	59.94	58.79	76.49	75.16	57.47	57.45	52.34	49.18	25.62	24.86	82.62	82.75	63.05	64.27
w/ VRE+ ℓ^2 -spa.	56.29	56.29	67.08	65.36	78.23	78.15	65.89	65.98	52.60	49.32	28.93	28.46	82.84	83.03	63.24	64.57
w/ VRE+KL-spa.	59.49	60.46	70.59	70.57	81.14	81.05	68.47	69.70	55.25	55.51	29.53	30.23	81.73	83.79	64.87	66.62
w/o Projector	59.07	60.43	70.41	71.24	81.28	81.01	68.49	70.09	55.64	55.98	30.06	31.30	83.18	85.44	65.88	68.73
w/ VRE+VCC	60.00	61.42	71.32	72.49	82.18	82.16	69.26	71.02	56.73	57.47	31.06	32.15	84.12	86.40	66.75	69.36

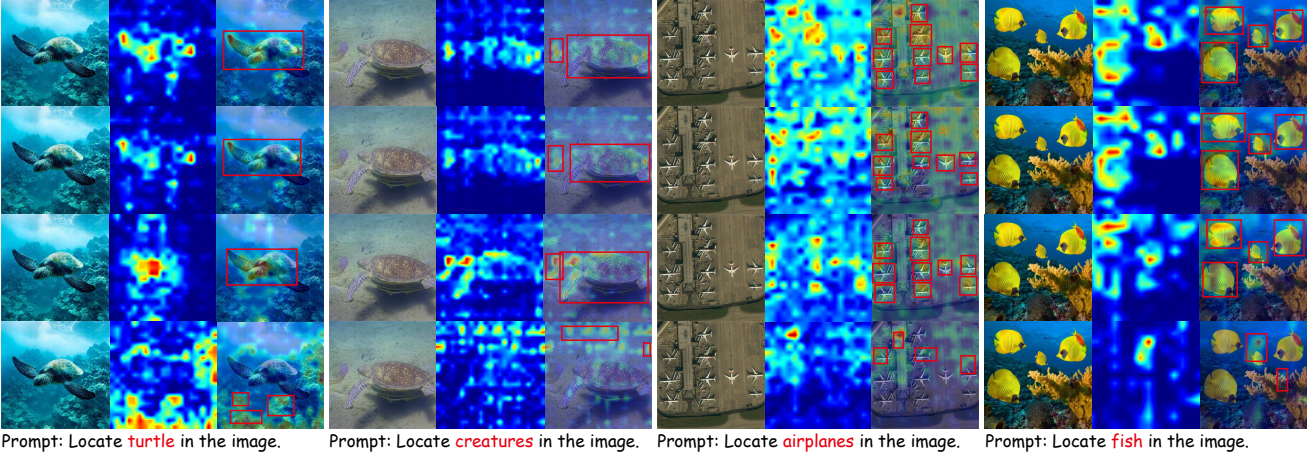


Figure 7. Visualization comparisons between UNIFER and Finetune. Row 1 and 2 of each group denote the visualization comparisons of UNIFER before and after it learns a new scenario. Row 3 and 4 of each group denote the visualization comparisons of Finetune before and after it learns a new scenario.

tigate the continual learning capabilities in cross scenarios of various methodologies. The model undergoes sequential training on two different scenarios. We then evaluate its performance on both seen and novel scenarios. Fig. 6 shows the results of the switching scenario (Underwater→Indoor/Indoor→Underwater) and the switching perspective (High altitude→Low altitude/Low altitude→High altitude). Both comparisons demonstrate that the proposed **UNIFER achieves a better trade-off between the seen and novel scenarios**, while most of other CL approaches show a significant performance decrease in the seen scenario.

4.3. Ablation Study and Analysis

Ablation study. We perform a detailed ablation study in Tab. 3. Row 1 reports the results of the baseline, which fine-tunes the model without any strategies. Row 2 adds a VRE structure on the baseline and Row 7 adds the VCC constraint on Row 2. Comparison of rows 1, 2 and 7 illustrates that each component of UNIFER effectively improves the model’s ability to resist forgetting.

Rows 3 to 6 show some alternatives to the structure or loss design. Row 3 is the simplest design as an alternative to Eq. (8), which constrains the intermediate represen-

tations using ℓ^2 -distance without channel reduction. And row 4 uses a channel reduction based on row 3 to penalize only global changes. The comparison shows that **looser constraints better balance between stability and plasticity**. Row 5 outperforms row 4 by replacing ℓ^2 -distance with relative entropy to use soft logits to constrain the representations of different scenarios. Row 6 shows the results of removing the projector. Although feature alignment maintains the representation consistency between the new and old models, simple feature addition constrains the model capacity to learn the new scenario. The comparison shows that **the projection layer is effective**.

Visualizations. Fig. 7 shows the visualizations of UNIFER and Finetune. Comparison between rows 1 and 2 of each group demonstrates that UNIFER maintains a stable representation of the old scenario throughout learning a new scenario, with attentional shifts confined to only a few regions. Therefore, the proposed method exhibits only minor missed detections and bounding box offsets after adaptation to new scenes. However, visualization of the Finetune shows that its attention undergoes a significant shift to some unrelated areas after learning a new scenario, which leads to a large number of false alarms and missed detections.

5. Conclusion

Multimodal continual learning is a key step in achieving a continual AI system. We propose multimodal continual learning with MLLMs from multi-scenario perspectives (UNIFIER). Specifically, we first propose a multimodal visual understanding dataset (**MSVQA**) to investigate catastrophic forgetting during complex visual grounding tasks under varying scenarios. Then, the proposed method introduces a dedicated branch for each scenario to keep their parameters independent. A vision consistency constraint is added to align the representations of different scenarios and thereby alleviate catastrophic forgetting. Extensive experiments validate the effectiveness of UNIFIER.

References

[1] Rahaf Aljundi, Punarjay Chakravarty, and Tinne Tuytelaars. Expert gate: Lifelong learning with a network of experts. In *Proceedings of the IEEE conference on computer vision and pattern recognition*, pages 3366–3375, 2017. 3, 6, 7, 5

[2] Stanislaw Antol, Aishwarya Agrawal, Jiasen Lu, Margaret Mitchell, Dhruv Batra, C Lawrence Zitnick, and Devi Parikh. Vqa: Visual question answering. In *Proceedings of the IEEE international conference on computer vision*, pages 2425–2433, 2015. 2

[3] Arjun Ashok, KJ Joseph, and Vineeth N Balasubramanian. Class-incremental learning with cross-space clustering and controlled transfer. In *European conference on computer vision*, pages 105–122. Springer, 2022. 5

[4] Yoshua Bengio, Aaron Courville, and Pascal Vincent. Representation learning: A review and new perspectives. *IEEE Transactions on Pattern Analysis and Machine Intelligence*, 35(8):1798–1828, 2013. 3

[5] Arslan Chaudhry, Marcus Rohrbach, Mohamed Elhoseiny, Thalaiyasingam Ajanthan, P Dokania, P Torr, and M Ranzato. Continual learning with tiny episodic memories. In *Workshop on Multi-Task and Lifelong Reinforcement Learning*, 2019. 6, 7, 5

[6] Fu Chenping, Liu Risheng, Fan Xin, Chen Puyang, Fu Hao, Yuan Wanqi, Zhu Ming, and Luo Zhongxuan. Rethinking general underwater object detection: Datasets, challenges, and solutions. *Neurocomputing*, 2023. 2

[7] Dima Damen, Hazel Doughty, Giovanni Maria Farinella, Sanja Fidler, Antonino Furnari, Evangelos Kazakos, Davide Moltisanti, Jonathan Munro, Toby Perrett, Will Price, and Michael Wray. Scaling egocentric vision: The epic-kitchens dataset. In *European Conference on Computer Vision (ECCV)*, 2018. 3

[8] Matthias De Lange, Rahaf Aljundi, Marc Masana, Sarah Parisot, Xu Jia, Aleš Leonardis, Gregory Slabaugh, and Tinne Tuytelaars. A continual learning survey: Defying forgetting in classification tasks. *IEEE Transactions on Pattern Analysis and Machine Intelligence*, 44(7):3366–3385, 2022. 1

[9] Arthur Douillard, Matthieu Cord, Charles Ollion, Thomas Robert, and Eduardo Valle. Podnet: Pooled outputs distillation for small-tasks incremental learning. In *European Conference on Computer Vision*, pages 86–102. Springer, 2020. 5, 6, 7

[10] Robert M French. Catastrophic forgetting in connectionist networks. *Trends in cognitive sciences*, 3(4):128–135, 1999. 1

[11] Nathan Godey, Éric Clergerie, and Benoît Sagot. Anisotropy is inherent to self-attention in transformers. In *Proceedings of the 18th Conference of the European Chapter of the Association for Computational Linguistics (Volume 1: Long Papers)*, pages 35–48, 2024. 5

[12] Haoran Gu, Handing Wang, Yi Mei, Mengjie Zhang, and Yaochu Jin. One trigger token is enough: A defense strategy for balancing safety and usability in large language models. *arXiv preprint arXiv:2505.07167*, 2025. 3

[13] Haoran Gu, Handing Wang, Yi Mei, Mengjie Zhang, and Yaochu Jin. Paretohqd: Fast offline multiobjective alignment of large language models using pareto high-quality data. *arXiv preprint arXiv:2504.16628*, 2025. 2

[14] Zhenyu Gu, Yanchen Xu, Sida Huang, Yubin Guo, and Hongyuan Zhang. Rectified noise: A generative model using positive-incentive noise. In *AAAI*, 2026. 2, 3

[15] Edward J Hu, Yelong Shen, Phillip Wallis, Zeyuan Allen-Zhu, Yuanzhi Li, Shean Wang, Lu Wang, Weizhu Chen, et al. Lora: Low-rank adaptation of large language models. *ICLR*, 1(2):3, 2022. 3

[16] Zhiyuan Hu, Yunsheng Li, Jiancheng Lyu, Dashan Gao, and Nuno Vasconcelos. Dense network expansion for class incremental learning. In *Proceedings of the IEEE/CVF Conference on Computer Vision and Pattern Recognition*, pages 11858–11867, 2023. 4

[17] Siqi Huang, Yanchen Xu, Hongyuan Zhang, and Xuelong Li. Learn beneficial noise as graph augmentation. In *ICML*, 2025. 3

[18] Sida Huang, Hongyuan Zhang, and Xuelong Li. Enhance vision-language alignment with noise. In *AAAI*, 2025. 3

[19] Sida Huang, Siqi Huang, Ping Luo, and Hongyuan Zhang. Laytrol: Preserving pretrained knowledge in layout control for multimodal diffusion transformers. In *AAAI*, 2026. 1

[20] Siqi Huang, Sida Huang, and Hongyuan Zhang. Colm: Collaborative large models via a client-server paradigm. In *AAAI*, 2026. 1

[21] Zhihao Huang, Xi Qiu, Yukuo Ma, Yifu Zhou, Junjie Chen, Hongyuan Zhang, Chi Zhang, and Xuelong Li. Nfig: Multi-scale autoregressive image generation via frequency ordering. In *The Thirty-ninth Annual Conference on Neural Information Processing Systems*, 2025. 2

[22] Saurav Jha, Dong Gong, and Lina Yao. Clap4clip: Continual learning with probabilistic finetuning for vision-language models. *Advances in neural information processing systems*, 37:129146–129186, 2024. 3

[23] Kai Jiang, Xueru Bai, and Feng Zhou. Recurrent network expansion for class incremental learning. *IEEE Transactions on Neural Networks and Learning Systems*, pages 1–14, 2025. 1, 4, 5, 6

[24] Kai Jiang, Zhengyan Shi, Dell Zhang, Hongyuan Zhang, and Xuelong Li. Mixture of noise for pre-trained model-based

class-incremental learning. *Advances in Neural Information Processing Systems*, 2025. 3

[25] James Kirkpatrick, Razvan Pascanu, Neil Rabinowitz, Joel Veness, Guillaume Desjardins, Andrei A Rusu, Kieran Milan, John Quan, Tiago Ramalho, Agnieszka Grabska-Barwinska, et al. Overcoming catastrophic forgetting in neural networks. *Proceedings of the national academy of sciences*, 114(13):3521–3526, 2017. 1

[26] Jiayi Kuang, Ying Shen, Jingyou Xie, Haohao Luo, Zhe Xu, Ronghao Li, Yinghui Li, Xianfeng Cheng, Xika Lin, and Yu Han. Natural language understanding and inference with mllm in visual question answering: A survey. *ACM Computing Surveys*, 57(8):1–36, 2025. 2

[27] Xuelong Li. Positive-incentive noise. *IEEE Transactions on Neural Networks and Learning Systems*, 35(6):8708–8714, 2024. 2

[28] Zhizhong Li and Derek Hoiem. Learning without forgetting. *IEEE Transactions on Pattern Analysis and Machine Intelligence*, 40(12):2935–2947, 2017. 3, 6

[29] Chang Liu, Yinpeng Dong, Wenzhao Xiang, Xiao Yang, Hang Su, Jun Zhu, Yuefeng Chen, Yuan He, Hui Xue, and Shibao Zheng. A comprehensive study on robustness of image classification models: Benchmarking and rethinking. *International Journal of Computer Vision*, 133(2):567–589, 2025. 1

[30] Haotian Liu, Chunyuan Li, Qingyang Wu, and Yong Jae Lee. Visual instruction tuning. *Advances in neural information processing systems*, 36:34892–34916, 2023. 3

[31] Zheda Mai, Ruiwen Li, Jihwan Jeong, David Quispie, Hyunwoo Kim, and Scott Sanner. Online continual learning in image classification: An empirical survey. *Neurocomputing*, 469:28–51, 2022. 1

[32] Imad Eddine Marouf, Enzo Tartaglione, Stéphane Lathuilière, and Joost van de Weijer. Ask and remember: A questions-only replay strategy for continual visual question answering. In *Proceedings of the IEEE/CVF International Conference on Computer Vision (ICCV)*, 2025. 2, 3, 4, 5, 6, 7

[33] Marc Masana, Xialei Liu, Bartłomiej Twardowski, Mikel Menta, Andrew D Bagdanov, and Joost Van De Weijer. Class-incremental learning: survey and performance evaluation on image classification. *IEEE Transactions on Pattern Analysis and Machine Intelligence*, 45(5):5513–5533, 2022. 1

[34] Francesco Pelosin, Saurav Jha, Andrea Torsello, Bogdan Raducanu, and Joost van de Weijer. Towards exemplar-free continual learning in vision transformers: an account of attention, functional and weight regularization. In *Proceedings of the IEEE/CVF Conference on Computer Vision and Pattern Recognition*, pages 3820–3829, 2022. 5

[35] Alec Radford, Jong Wook Kim, Chris Hallacy, Aditya Ramesh, Gabriel Goh, Sandhini Agarwal, Girish Sastry, Amanda Askell, Pamela Mishkin, Jack Clark, et al. Learning transferable visual models from natural language supervision. In *International conference on machine learning*, pages 8748–8763. PMLR, 2021. 3

[36] Sylvestre-Alvise Rebuffi, Alexander Kolesnikov, Georg Sperl, and Christoph H Lampert. icarl: Incremental classifier and representation learning. In *Proceedings of the IEEE conference on Computer Vision and Pattern Recognition*, pages 2001–2010, 2017. 3

[37] Xian Sun, Peijin Wang, Zhiyuan Yan, Feng Xu, Ruiping Wang, Wenhui Diao, Jin Chen, Jihao Li, Yingchao Feng, and Tao Xu. Fair1m: A benchmark dataset for fine-grained object recognition in high-resolution remote sensing imagery. *ISPRS Journal of Photogrammetry and Remote Sensing*, 184, 2022. 1

[38] Ashish Vaswani, Noam Shazeer, Niki Parmar, Jakob Uszkoreit, Llion Jones, Aidan N Gomez, Łukasz Kaiser, and Illia Polosukhin. Attention is all you need. *arXiv*, 2017. 3

[39] Elena Voita, David Talbot, Fedor Moiseev, Rico Sennrich, and Ivan Titov. Analyzing multi-head self-attention: Specialized heads do the heavy lifting, the rest can be pruned. In *57th Annual Meeting of the Association for Computational Linguistics*, pages 5797–5808. ACL Anthology, 2019. 5

[40] Liyuan Wang, Xingxing Zhang, Hang Su, and Jun Zhu. A comprehensive survey of continual learning: Theory, method and application. *IEEE Transactions on Pattern Analysis and Machine Intelligence*, 2024. 1

[41] Peng Wang, Shuai Bai, Sinan Tan, Shijie Wang, Zhihao Fan, Jinze Bai, Keqin Chen, Xuejing Liu, Jialin Wang, Wenbin Ge, et al. Qwen2-vl: Enhancing vision-language model’s perception of the world at any resolution. *arXiv preprint arXiv:2409.12191*, 2024. 3

[42] Zihan Wang, Jiuxiang Gu, Jason Kuen, Handong Zhao, Vlad Morariu, Ruiyi Zhang, Ani Nenkova, Tong Sun, and Jingbo Shang. Learning adaptive axis attentions in fine-tuning: Beyond fixed sparse attention patterns. In *Findings of the Association for Computational Linguistics: ACL 2022*, pages 916–925, 2022. 5

[43] Yangyang Xu, Yibo Yang, and Lefei Zhang. Multi-task learning with knowledge distillation for dense prediction. In *Proceedings of the IEEE/CVF International Conference on Computer Vision*, pages 21550–21559, 2023. 5

[44] Shipeng Yan, Jiangwei Xie, and Xuming He. Der: Dynamically expandable representation for class incremental learning. In *Proceedings of the IEEE/CVF Conference on Computer Vision and Pattern Recognition*, pages 3014–3023, 2021. 4

[45] Dianzhi Yu, Xinni Zhang, Yankai Chen, Aiwei Liu, Yifei Zhang, Philip S Yu, and Irwin King. Recent advances of multimodal continual learning: A comprehensive survey. *arXiv preprint arXiv:2410.05352*, 2024. 2

[46] Yuan Yuan, Zhaojian Li, and Bin Zhao. A survey of multimodal learning: Methods, applications, and future. *ACM Computing Surveys*, 57(7):1–34, 2025. 2

[47] Hongyuan Zhang, Yanchen Xu, Sida Huang, and Xuelong Li. Data augmentation of contrastive learning is estimating positive-incentive noise. *arXiv preprint arXiv:2408.09929*, 2024. 3

[48] H Zhang, S Huang, Y Guo, and X Li. Variational positive-incentive noise: How noise benefits models. *IEEE TPAMI*, 2025. 2

[49] Xi Zhang, Feifei Zhang, and Changsheng Xu. Vqacl: A novel visual question answering continual learning setting.

In *Proceedings of the IEEE/CVF Conference on Computer Vision and Pattern Recognition*, pages 19102–19112, 2023.
2, 3, 6, 7, 5

- [50] Da-Wei Zhou, Hai-Long Sun, Han-Jia Ye, and De-Chuan Zhan. Expandable subspace ensemble for pre-trained model-based class-incremental learning. In *Proceedings of the IEEE/CVF Conference on Computer Vision and Pattern Recognition*, pages 23554–23564, 2024. 4, 6
- [51] Da-Wei Zhou, Zi-Wen Cai, Han-Jia Ye, De-Chuan Zhan, and Ziwei Liu. Revisiting class-incremental learning with pre-trained models: Generalizability and adaptivity are all you need. *International Journal of Computer Vision*, 133(3):1012–1032, 2025. 1
- [52] Didi Zhu, Zhongyisun Sun, Zexi Li, Tao Shen, Ke Yan, Shouhong Ding, Chao Wu, and Kun Kuang. Model tailor: Mitigating catastrophic forgetting in multi-modal large language models. In *International Conference on Machine Learning*, pages 62581–62598. PMLR, 2024. 3, 6, 7, 5
- [53] Pengfei Zhu, Longyin Wen, Dawei Du, Xiao Bian, Heng Fan, Qinghua Hu, and Haibin Ling. Detection and tracking meet drones challenge. *IEEE Transactions on Pattern Analysis and Machine Intelligence*, 44(11):7380–7399, 2021. 2
- [54] Ruishu Zhu, Sida Huang, Ziheng Jiao, and Hongyuan Zhang. Explore how to inject beneficial noise in mllms. In *AAAI*, 2026. 1
- [55] Yongshuo Zong, Oisin Mac Aodha, and Timothy M Hospedales. Self-supervised multimodal learning: A survey. *IEEE Transactions on Pattern Analysis and Machine Intelligence*, 47(7):5299–5318, 2024. 2
- [56] Zhengxia Zou, Keyan Chen, Zhenwei Shi, Yuhong Guo, and Jieping Ye. Object detection in 20 years: A survey. *Proceedings of the IEEE*, 111(3):257–276, 2023. 6

Multimodal Continual Learning with MLLMs from Multi-scenario Perspectives

Supplementary Material

A. Overview

In this supplementary material, we provide more details about UNIFIER. We first introduce details of the multimodal visual understanding dataset MSVQA (in Sec. B) and provide the corresponding evaluation metrics (in Sec. C). Then, we provide descriptions of all comparison methods (in Sec. D). Moreover, we provide the hardware information for all experiments and summarize the computational resource requirements with complexity analysis (in Sec. E). Furthermore, we compare the upper bounds of Qwen2.5VL-3B, Qwen2.5VL-7B and Qwen3VL-4B to investigate the influence of different model sizes and foundation models in Sec. F, which detailed experiments on setting of 10 steps using Qwen3VL-4B are performed in Sec. G. Finally, we provide complete comparison experiments (in Sec. H) and complete scenario alteration experiments (in Sec. I).

B. Dataset details

B.1. High altitude.

The source data of high altitude scenario are from a large-scale optical remote sensing dataset [37].

Data Preprocess: We mainly execute four operations.

1. Separate image containing airports from the source data.
2. Perform sliding window cropping on high-resolution images to ensure that the maximum size of the image slices does not exceed 1500 pixels, and set the backtracking step size to 200 pixels to ensure that each target appears completely in at least one slice.
3. Recalculate the coordinates for each target using the

cropping parameters.

4. Transform coordinate data into a standard format and populate a JSON file accordingly with the designed VQA template.

Fig. A1 presents data from high altitude scenarios, comprising five types of question, i.e., Counting, Classification, True or False, Visual Grounding, and Fine-grained Visual Grounding.

Easy visual tasks:

1. **Counting:** Determine the number of airplanes in the input image (Maximum ≥ 30).
2. **Classification:** Determine the aircraft models presented in the image. A set of aircraft models is provided in the question (orange text) as prior knowledge. MLLM is required to comprehend aircraft models associated with the image from the training data and to indicate the specific models shown in the image.
3. **True or False:** Determine whether there is a specific aircraft model in the image. MLLM needs to first extract the specific aircraft model from the query, then assess whether that aircraft model is present in the input image, and finally output a standard response of 'yes' or 'no'.

Complex visual tasks:

1. **Visual Grounding:** Locate all the airplanes in the input image and then output the rectangular coordinates in LIST format. This requires MLLMs to accurately interpret the query and locate the target precisely within the image. Precise localization capability is a critical step for MLLMs in practical applications.
2. **Visual Grounding (fine-grained):** Locate the specified airplane model in the image and output the bounding box coordinates in LIST format. In contrast to task 4,

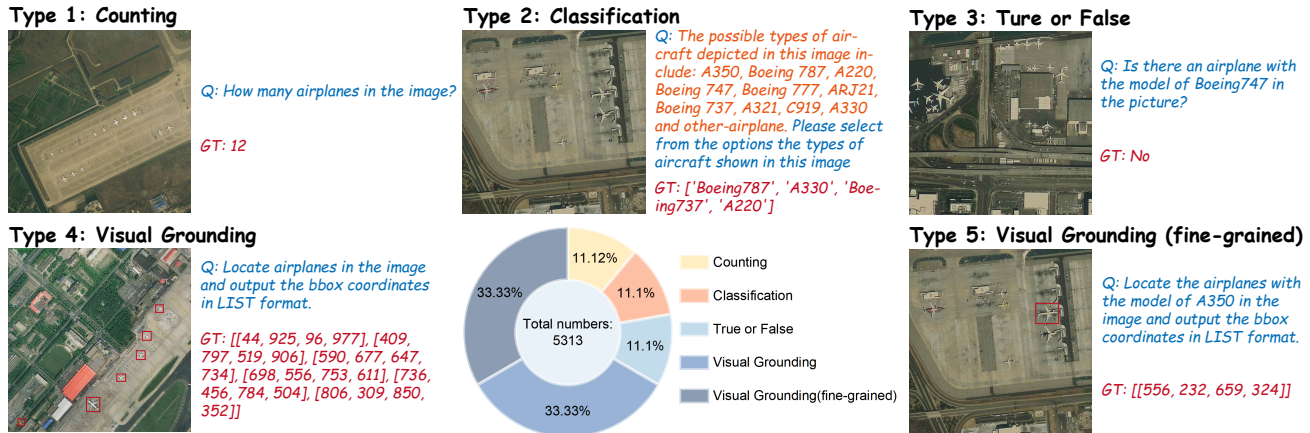


Figure A1. Illustrations of high altitude data.

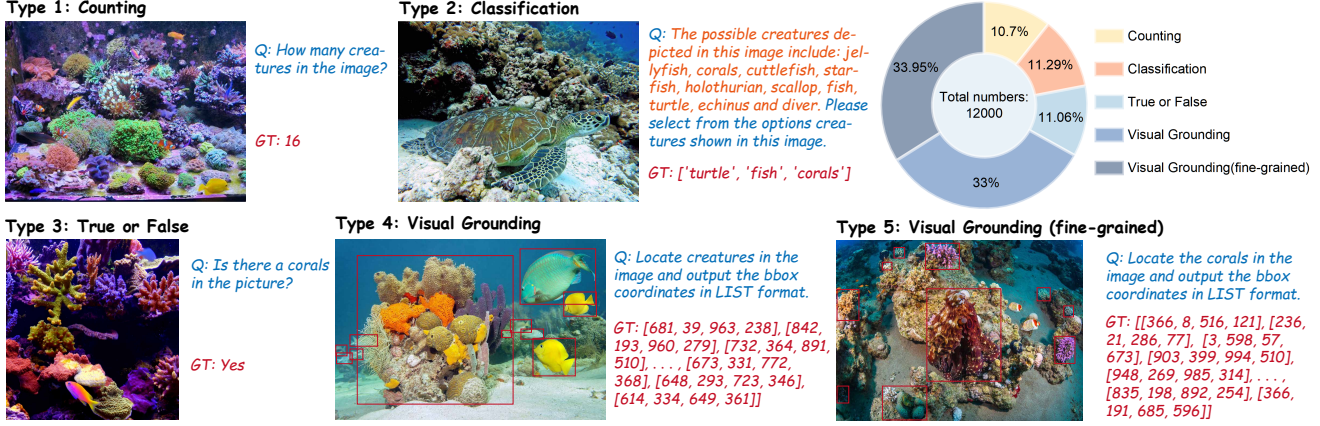


Figure A2. Illustrations of underwater data.

the fine-grained detection task requires MLLMs to accurately identify the target airplane model and exhibits fine-grained classification capabilities. The small size of the targets makes fine-grained detection particularly challenging.

B.2. Underwater

The source data of underwater scenario are from [6].

Data Preprocess: We mainly execute three operations.

1. Perform adaptive scaling on the image to ensure that its dimensions are less than 1500×1500 pixels.
2. Adjust the coordinates of all targets according to the scaling parameters.
3. Transform coordinate data into a standard format and populate a JSON file accordingly with the designed VQA template.

Fig. A2 presents data from underwater scenarios, comprising five types of question, i.e., Counting, Classification, True or False, Visual Grounding, and Fine-grained Visual Grounding.

Easy visual tasks:

1. **Counting:** Determine the number of creatures in the input image (Maximum ≥ 80).
2. **Classification:** Determine the species presented in the image. A set of species is provided in the question (orange text) as prior knowledge. MLLM is required to comprehend the creatures associated with the image from the training data and to indicate the specific species shown in the image.
3. **True or False:** Determine whether there is a specific creature in the image. MLLM needs to first extract the specific creatures from the query, then assess whether that creature is present in the input image, and finally output a standard response of 'yes' or 'no'.

Complex visual tasks:

1. **Visual Grounding:** Locate all the creatures in the input image and then output the rectangular coordinates in

LIST format. Due to the light attenuation and scattering, as well as the camouflage colors of marine creatures, object detection in underwater scenario is highly challenging.

2. **Visual Grounding (fine-grained):** Locate the specified creature in the image and output the bounding box coordinates in LIST format. The diminutive size of certain marine organisms (such as echinus and fish) complicates the detection of such small targets against a complex background.

B.3. Low altitude

The source data of low altitude scenario are from [53].

Data Preprocess: We mainly execute three operations.

1. Perform adaptive scaling on the image to ensure that its dimensions are less than 1500×1500 pixels.
2. Adjust the coordinates of all targets according to the scaling parameters.
3. Transform coordinate data into a standard format and populate a JSON file accordingly with the designed VQA template.

Fig. A3 presents data from low altitude scenarios, comprising five types of question, i.e., Counting, Classification, True or False, Visual Grounding, and Fine-grained Visual Grounding.

Easy visual tasks:

1. **Counting:** Determine the number of vehicles and human in the input image (Maximum ≥ 80).
2. **Classification:** Determine the objects presented in the image. A set of objects is provided in the question (orange text) as prior knowledge. MLLM is required to comprehend the objects associated with the image from the training data and to indicate the specific vehicles (or human) shown in the image.
3. **True or False:** Determine whether there is a specific vehicle in the image. MLLM needs to first extract the specific vehicles from the query, then assess whether that

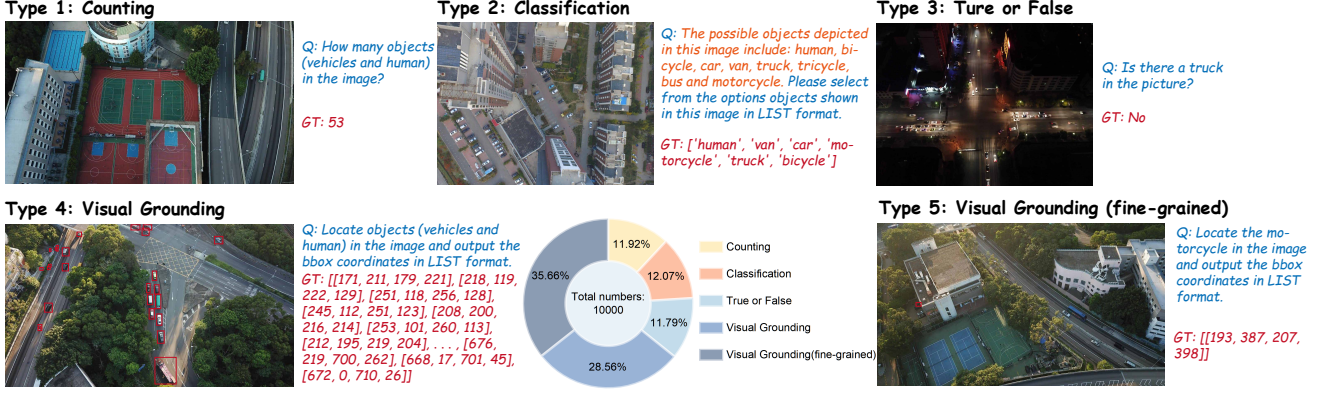


Figure A3. Illustrations of low altitude data.

vehicle is present in the input image, and finally output a standard response of 'yes' or 'no'.

Complex visual tasks:

1. **Visual Grounding:** Locate all the vehicles and human in the input image and then output the rectangular coordinates in LIST format. Target localization in low-altitude scenarios is challenging due to the small size of the targets and frequent obstructions.
2. **Visual Grounding (fine-grained):** Locate the specified vehicle in the image and output the bounding box coordinates in LIST format. Fine-grained targets are typically concealed within complex backgrounds and are frequently subject to severe overlap and occlusion, thereby complicating fine-grained localization.

B.4. Indoor

The source data for the indoor scenario are from a large-scale first-person video dataset [7].

Data Preprocess: We mainly execute four operations.

1. Extract key frames from the video stream and remove duplicate frames.
2. Perform adaptive scaling on the image to ensure that its dimensions are less than 1500×1500 pixels.
3. Adjust the coordinates of all targets according to the scaling parameters.
4. Transform coordinate data into a standard format and populate a JSON file accordingly with the designed VQA template.

Fig. A4 presents data from indoor scenarios, comprising two types of question, i.e., Action speculation and Visual Grounding.

Action speculation: is conducted through choice questions aimed at deducing the ongoing actions of the first-person protagonist. Each option is formed by pairing a verb (or verbal phrase) with a noun. The set of four options includes: one random action, one correct action, one option that uses the **correct verb** but an **incorrect noun**, and one option that uses the **correct noun** but an **incorrect verb**. The inclusion

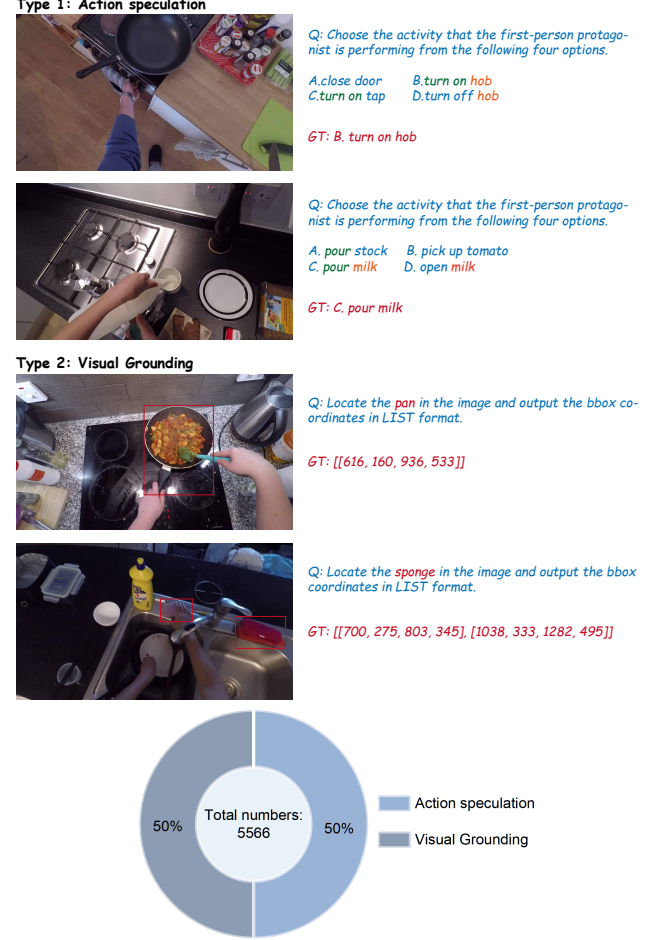


Figure A4. Illustrations of indoor data.

of these distractors ensures that the model must accurately interpret the character's action in the image, rather than relying solely on object recognition to choose the correct answer.

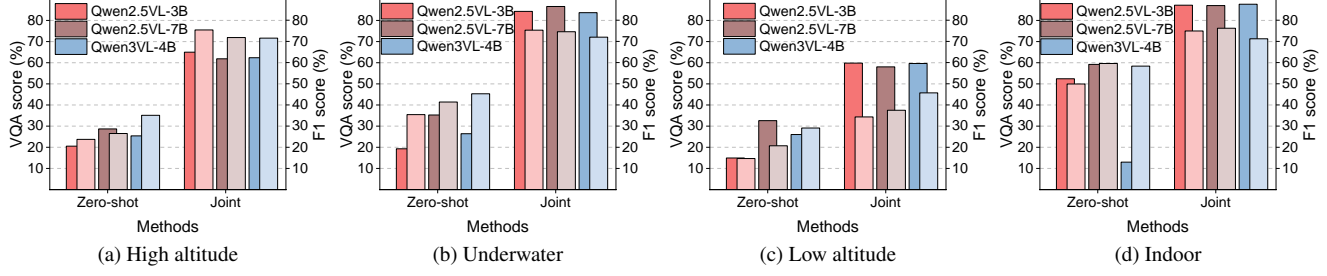


Figure A5. Comparison of Zero-shot and the upper bound between Qwen2.5VL-3B, Qwen2.5VL-7B and Qwen3VL-4B. The dark color corresponds to the VQA score, and the light color corresponds to the F1 score.

Visual Grounding: locates the common objects in the indoor scenario from the first-person perspective. Due to the constrained field of view inherent in the first-person perspective and the presence of optical distortions such as lens aberration and defocus, object detection within dynamic indoor scenario data streams is a significant challenge.

The data distribution in Fig. A1 to A4 indicates that MSVQA involves a significant proportion of complex visual grounding tasks, which imposes greater demands on the model’s visual reasoning abilities.

C. Evaluation metrics

C.1. VQA score

We compute the VQA score for each scenario by aggregating the scores from the Counting, Classification, True or False, and Action speculation tasks.

Counting. Due to the presence of small, numerous, and overlapping targets in certain scenarios, we allow the model to have a certain degree of prediction error. Consequently, 1 score is assigned if the predicted count exactly matches the ground truth, 0.5 score is given if the absolute difference between the predicted count and the ground truth is less than one, and no score is awarded otherwise.

Classification. We first compare the predicted results with the ground truth. Since the ground truth comprises multiple category labels, we can obtain the number of correct predictions n_{correct} and incorrect predictions n_{wrong} . Assume n_{all} denotes the sequence length of ground truth, the final score can be calculated by

$$\max \left(\frac{(n_{\text{correct}} - 0.5 \times n_{\text{wrong}})}{n_{\text{all}}}, 0 \right). \quad (\text{A1})$$

True or False. The score is determined by directly comparing the predictions with the ground truth, where a correct match yields 1 score.

Action speculation. The score is determined by directly comparing the predictions with the ground truth, where a correct match yields 1 score.

For high altitude, underwater, and low altitude scenarios, we compute the total scores for the Counting, Classification,

and True or False tasks individually, then normalize them to a percentage scale to derive the VQA score. For the indoor scenario, we calculate the total score for action speculation and similarly convert it to a percentage score as the VQA score.

C.2. F1 score

We adopt the F1 score to measure the visual grounding capacity of MLLMs. First, we collect the predicted bounding boxes for all images. Subsequently, these predictions are matched with ground truth boxes based on $\text{IoU} = 0.5$, allowing the calculation of true positives (TP), false positives (FP), and false negatives (FN). The precision is calculated by $\text{TP}/(\text{TP} + \text{FP})$ and the recall is calculated by $\text{TP}/(\text{TP} + \text{FN})$. The F1 score is defined as the harmonic mean of precision and recall,

$$\text{F1} = \frac{2 \times \text{Precision} \times \text{Recall}}{(\text{Precision} + \text{Recall})}. \quad (\text{A2})$$

In particular, the F1 score for visual grounding and fine-grained visual grounding tasks should be calculated separately for high altitude, underwater and low altitude scenarios. Therefore, the average of the F1 scores from two tasks is adopted to evaluate the performance of complex visual tasks in each scenario.

D. Comparison methods

We compared nine different methods, comprising zero-shot for pre-training capability, the lower bound (Finetune), the upper bound (Joint), two exemplar-free methods, and four exemplar-based methods. The descriptions of these methods are provided below.

- **Zero-shot:** aims to validate the performance from pre-training. It initializes the model with the pre-trained weight and then is validated on the test set. Due to the non-standard output by an untrained model, We analyzed the inference outputs and optimize the scoring algorithm by incorporating techniques such as fuzzy matching.
- **Joint:** is the upper bound of continual learning. It always learns both previous data and current data in each

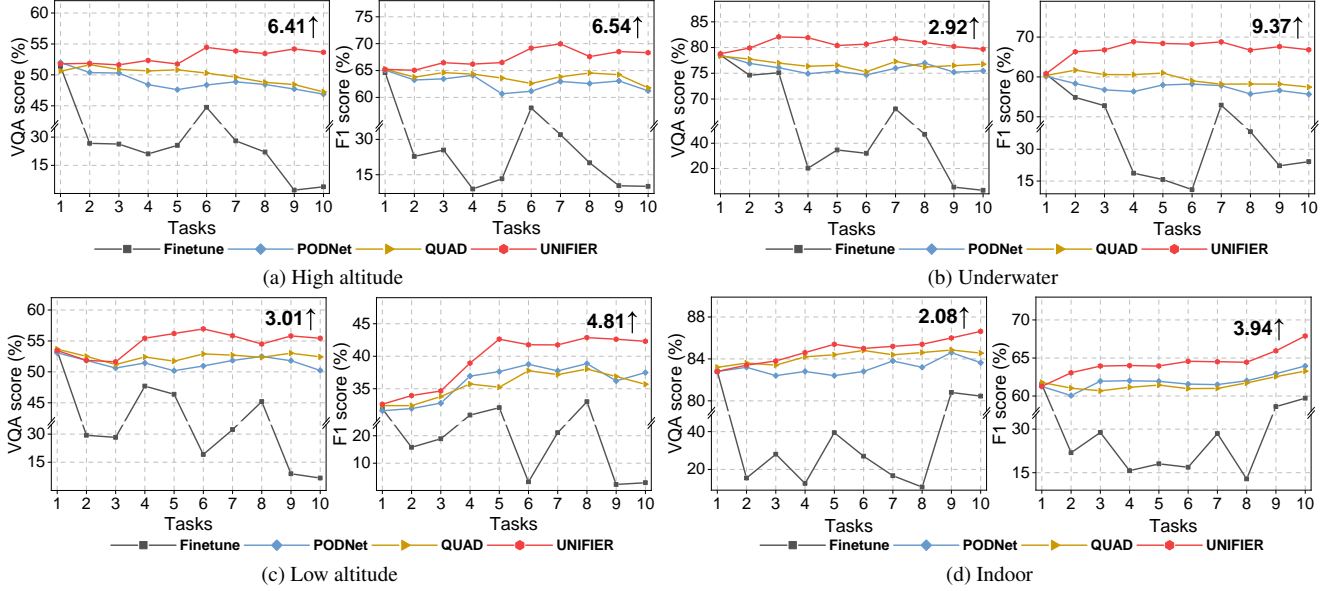


Figure A6. Incremental trends on 10 steps setting using **Qwen3-VL**. The performance gap is annotated at the end of each curve.

task jointly. However, it spends more training and storage cost.

- **Finetune**: is the lower bound of continual learning. It only learns current data without other strategies. Therefore, it suffers from severe catastrophic forgetting.
- **EWC** [1]: addresses catastrophic forgetting by selectively slowing the learning of important weights for previous tasks, using a regularization term based on the Fisher Information Matrix to constrain significant parameter changes. Its key advantage is effectively preserving performance on old tasks without storing past data, through a relatively simple and computationally efficient mechanism. However, EWC can be computationally expensive to compute the Fisher matrix for MLLMs.
- **Tailor** [52]: aims to mitigate catastrophic forgetting by identifying a sparse model patch of critical parameters through a fusion of salience and sensitivity analysis, followed by targeted compensation to enhance task adaptation. However, it exhibits limited performance in multi-scenario tasks due to substantial variations in visual features.
- **ER** [5]: is a rehearsal-based method that employs a fixed-size memory buffer to store and randomly sample visited examples for retraining.
- **PODNet** [9]: is also a rehearsal-based method that employs pooling operations across the dimensions of intermediate features to derive compressed representations for each dimension. It facilitates a trade-off between stability and plasticity by computing the L2 norm between the compressed representations of the old and new models. The original method is based on convolutional networks. We develop it to fit the ViT architecture.

- **VQACL** [49]: employs a rehearsal-based strategy that integrates a prototype module to capture both task-specific and invariant features, thereby enabling robust and generalizable representations for VQA tasks.
- **QUAD** [32]: employs a questions-only rehearsal strategy without storing visual data by leveraging previous task questions for regularization. It integrates question replay to prevent overfitting and attention consistency distillation to preserve cross-modal associations. However, it may underperform in tasks requiring detailed visual reasoning due to the absence of image storage.

E. Hardware and Complexity Analysis

The hardware information is as follows:

- **CPU**: Intel(R) XEON(R) PLATINUM 8558 (96 core)
- **GPU**: 8×NVIDIA H200 (140 GB per device)
- **Mem**: 500 GB

Using the setting of 10 steps as an example, we compare the training and inference costs of UNIFIER with those of other methods. With identical hardware (NVIDIA H200 GPUs), we quantified the total training costs for EWC, ER, QUAD, and UNIFIER on the given task. EWC consumes 41.47 GPUh, ER 35.87 GPUh, QUAD 48.67 GPUh, and UNIFIER only 32.67 GPUh. EWC needs preserve an information matrix similar in size to the original model during updates, substantially increasing the training cost. ER introduces a slight increase in training cost as a result of saving old samples. QUAD requires duplicate forward propagation to compute loss using intermediate features from the combination of old questions and new images, leading to higher training costs. In contrast, UNIFIER updates only a specific branch for visual encoder, resulting in reduced training

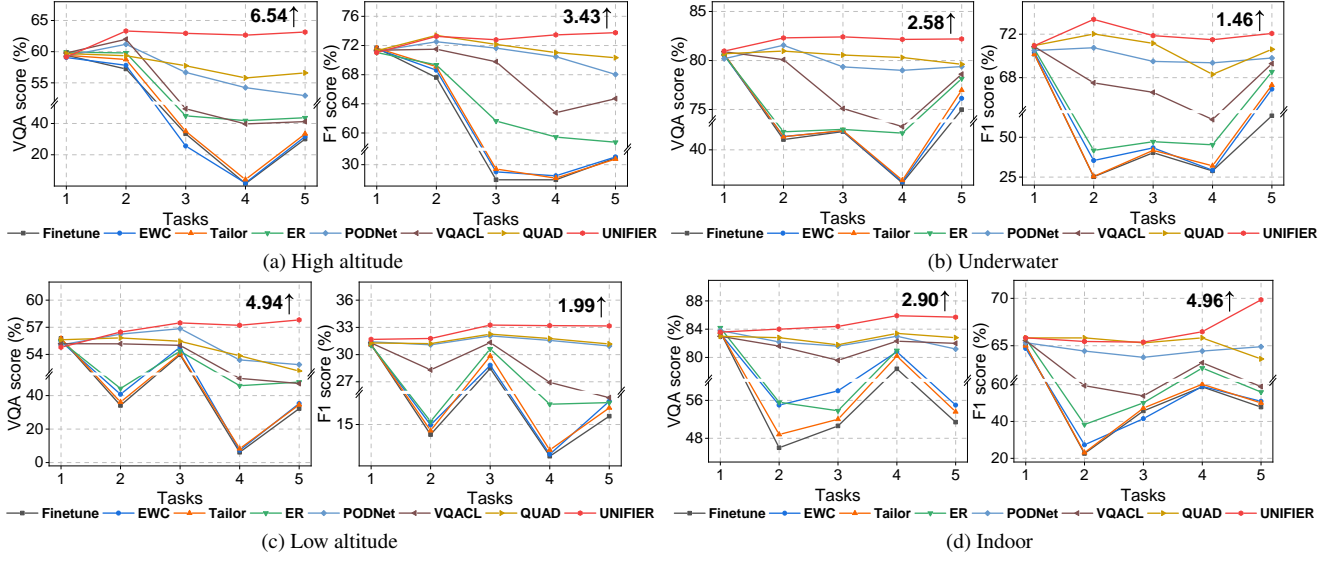


Figure A7. Incremental trends on 5 steps setting in different scenarios. The performance gap is annotated at the end of each curve.

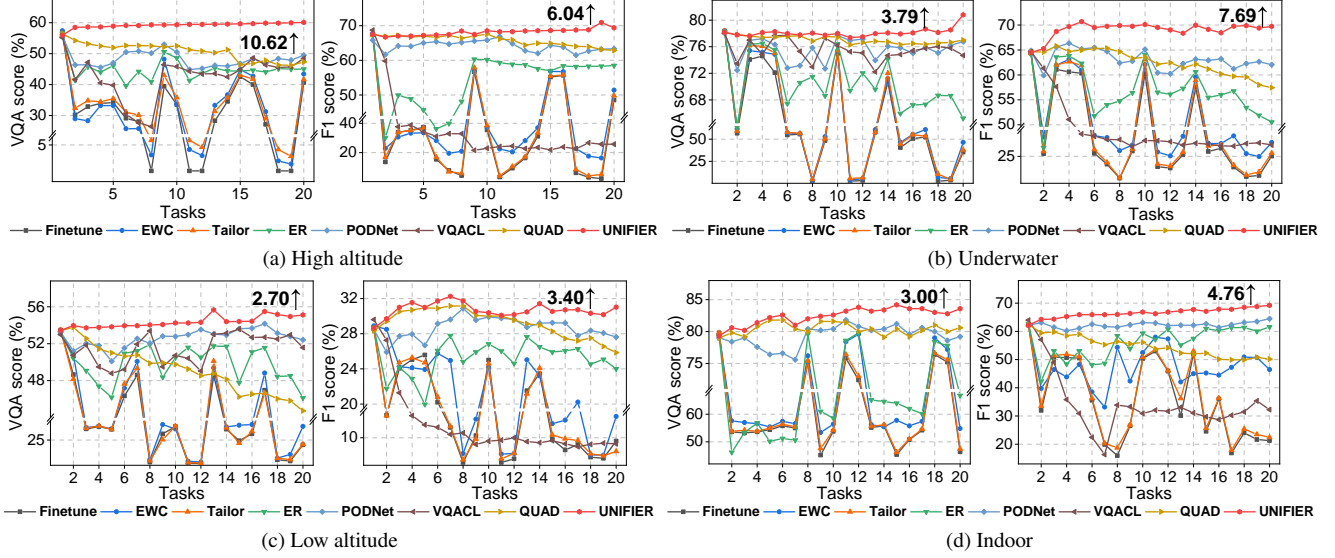


Figure A8. Incremental trends on 20 steps setting in different scenarios. The performance gap is annotated at the end of each curve.

costs.

Furthermore, we compare the inference cost of the UNIFIER and the baseline in the test set. The baseline method spends an average of 4.11 GPUh for a complete inference on the test set, while the proposed method spends 4.73 GPU hours after learning four scenarios. Therefore, the inference cost of the proposed method only increases by 15% compared to the baseline. Shows a better trade-off between training and inference cost, demonstrating the superiority of the proposed method in continual learning.

F. Comparison of different upper bounds

In this section, we perform additional experiments with Qwen2.5-VL-7B and Qwen3-VL-4B to eliminate the influence of different model types. All models are trained with

the same hyper-parameters by 20 epochs. The comparison is shown in Fig. A5. The results indicate that, although there is a slight disparity in the performance of zero-shot using these foundation models, their fine-tuned performance is comparable.

G. Further experiments with Qwen3-VL

To further investigate the generalization ability of the UNIFIER across various foundation models, we performed additional experiments with **Qwen3-VL**. The results for the setting of 10 steps are presented in Fig. A6. We compare the proposed method with QUAD, PODNet, and the lower bound Finetune, with the last-step VQA score of UNIFIER outperforming the runner up by 2.08%~6.41%, and the last-step F1 score outperforming the runner up by

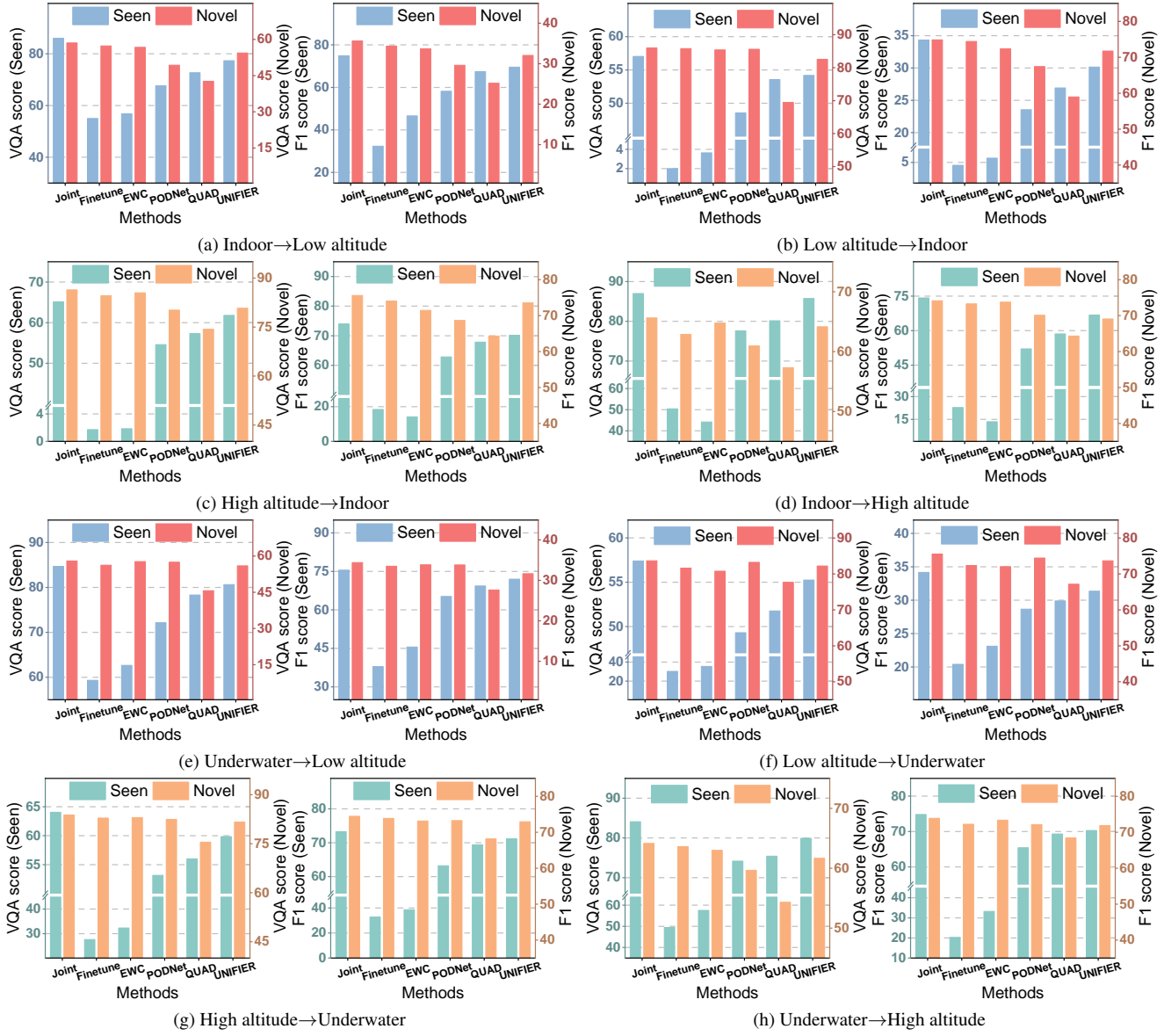


Figure A9. More experimental results of scenario alteration in one step.

3.94%~9.37%. It demonstrates that the UNIFIER is still effective with Qwen3-VL.

H. Comparison experiments

In this section, we provide the results of complete comparison experiments, including 5 steps in Fig. A7 and 20 steps in Fig. A8. The performance gap is annotated at the end of each curve. This indicates that the proposed method can effectively prevent catastrophic forgetting in various task settings.

I. Scenario alteration experiments

In this section, we provide more experiments on scenario alteration, including Indoor↔Low altitude (Fig. A9a

and A9b), High altitude↔Indoor (Fig. A9c and A9d), Underwater↔Low altitude (Fig. A9e and A9f) and High altitude↔Underwater (Fig. A9g and A9h). Experimental results demonstrate that the UNIFIER achieves better performance in continual learning across scenarios than comparison methods.